Neuron 45, 857–871, March 16, 2005 ©2005 Elsevier Inc. DOI 10.1016/j.neuron.2005.02.019

Blanes Cells Mediate Persistent Feedforward Inhibition onto Granule Cells in the Olfactory Bulb

R. Todd Pressler[1] and Ben W. Strowbridge[1,*]
[1] Department of Neurosciences
Case Western Reserve University
Cleveland, Ohio 44106

Summary

Inhibitory local circuits in the olfactory bulb play a critical role in determining the firing patterns of output neurons. However, little is known about the circuitry in the major plexiform layers of the olfactory bulb that regulate this output. Here we report the first electrophysiological recordings from Blanes cells, large stellate-shaped interneurons located in the granule cell layer. We find that Blanes cells are GABAergic and generate large I_{CAN}-mediated afterdepolarizations following bursts of action potentials. Using paired two-photon guided intracellular recordings, we show that Blanes cells have a presumptive axon and monosynaptically inhibit granule cells. Sensory axon stimulation evokes barrages of EPSPs in Blanes cells that trigger long epochs of persistent spiking; this firing mode was reset by hyperpolarizing membrane potential steps. Persistent firing in Blanes cells may represent a novel mechanism for encoding short-term olfactory information through modulation of tonic inhibitory synaptic input onto bulbar neurons.

Introduction

Local circuits are the fundamental building blocks that define how different CNS regions process afferent information. Local circuits often are described in terms of specific patterns of synaptic interactions (e.g., feedback and feedforward inhibition, recurrent excitation, lateral inhibition) that are iterated across modules within a brain region (Douglas and Martin, 1991; Shepherd and Greer, 1998; Stepanyants et al., 2004). In the olfactory bulb, the second-order olfactory brain region, sensory information is relayed from olfactory receptor neurons to both principal neurons (mitral and tufted cells) and to a variety of glomerular-layer interneurons (Shepherd and Greer, 1998). The computational work of the olfactory bulb presumably is mediated in large part by stereotyped synaptic interactions that take place in the inner and outer plexiform layers and that are replicated in the local circuits linked to the ~1800 olfactory glomeruli that receive olfactory receptor subtype specific afferents (Mori et al., 1999; Shepherd and Greer, 1998). However, little is known about the local circuits that operate in these plexiform and output layers of the olfactory bulb, aside from the reciprocal dendrodendritic synapse formed between mitral cells and axonless granule cells (Jahr and Nicoll, 1980; Price and Powell, 1970b; Rall and Shepherd, 1968). This dendritic microcircuit mediates both feedback and lateral inhibition (Isaacson and Strowbridge, 1998; Schoppa et al., 1998) of mitral cells but is strongly dependent on NMDAR activation and therefore is tonically attenuated by extracellular Mg ions. Conventional inhibitory local circuits that involve transmitter release from axon terminals have not been demonstrated electrophysiologically in the major plexiform layers of the olfactory bulb.

This paucity of functional data regarding the local circuitry in most of the olfactory bulb contrasts with the abundance of anatomical data that demonstrates the presence of a wide variety of presumptive interneurons in this brain region. In the granule cell layer alone, at least seven types of non-granule cells have been demonstrated using Golgi and immunocytochemical methods (Alonso et al., 2001; Kakuta et al., 1998; Lopez-Mascaraque et al., 1986; Schneider and Macrides, 1978). The electrophysiological properties and synaptic connections made by these interneurons have not been explored previously. Recent work on interneuronal subtypes in the glomerular input layer (Aungst et al., 2003) has significantly revised the canonical basic circuit for the olfactory bulb, which now includes long-range (interglomerular) excitatory synaptic projections made by so-called "short axon" cells. Understanding the functional consequences of interneuronal diversity in the olfactory bulb is a critical step toward the goal of deciphering the computational operations performed by this major brain region.

In this study we sought to define the properties and synaptic connections made by one subpopulation of interneurons that is readily identifiable under infrared differential interference contrast (IR-DIC) microscopy: large stellate-shaped neurons in the granule cell layer. We used whole-cell patch-clamp recording and two-photon imaging in acute brain slices to determine whether these cells represent a novel cell type that is anatomically and electrophysiologically distinct from granule cells. We found that these stellate-shaped cells are a GABAergic cell type that innervate granule cells and generate large depolarizing afterpotentials following transient stimulation. We refer to these neurons as "Blanes cells," reflecting their morphological similarity to cells first described in Golgi-stained olfactory bulb sections (Blanes, 1898). We found that brief depolarizing stimuli trigger persistent activity in Blanes cells that can be reset by membrane potential hyperpolarization. Persistent spiking in Blanes cells is a previously unrecognized feature of the olfactory bulb and may represent an intrinsic form of short-term memory that enables brief sensory experiences to modulate activity in local circuits over a time span of seconds to minutes.

Results

In addition to granule cells, IR-DIC microscopy revealed other neurons in the granule cell layer of rat olfactory bulb slice with cell bodies that are much larger than granule cells (mean size viewed under IR-DIC illumination = 20.0 × 12.6 μm for large cells and 11.8 × 9.7 μm for granule cells). A subpopulation of these large

*Correspondence: bens@case.edu

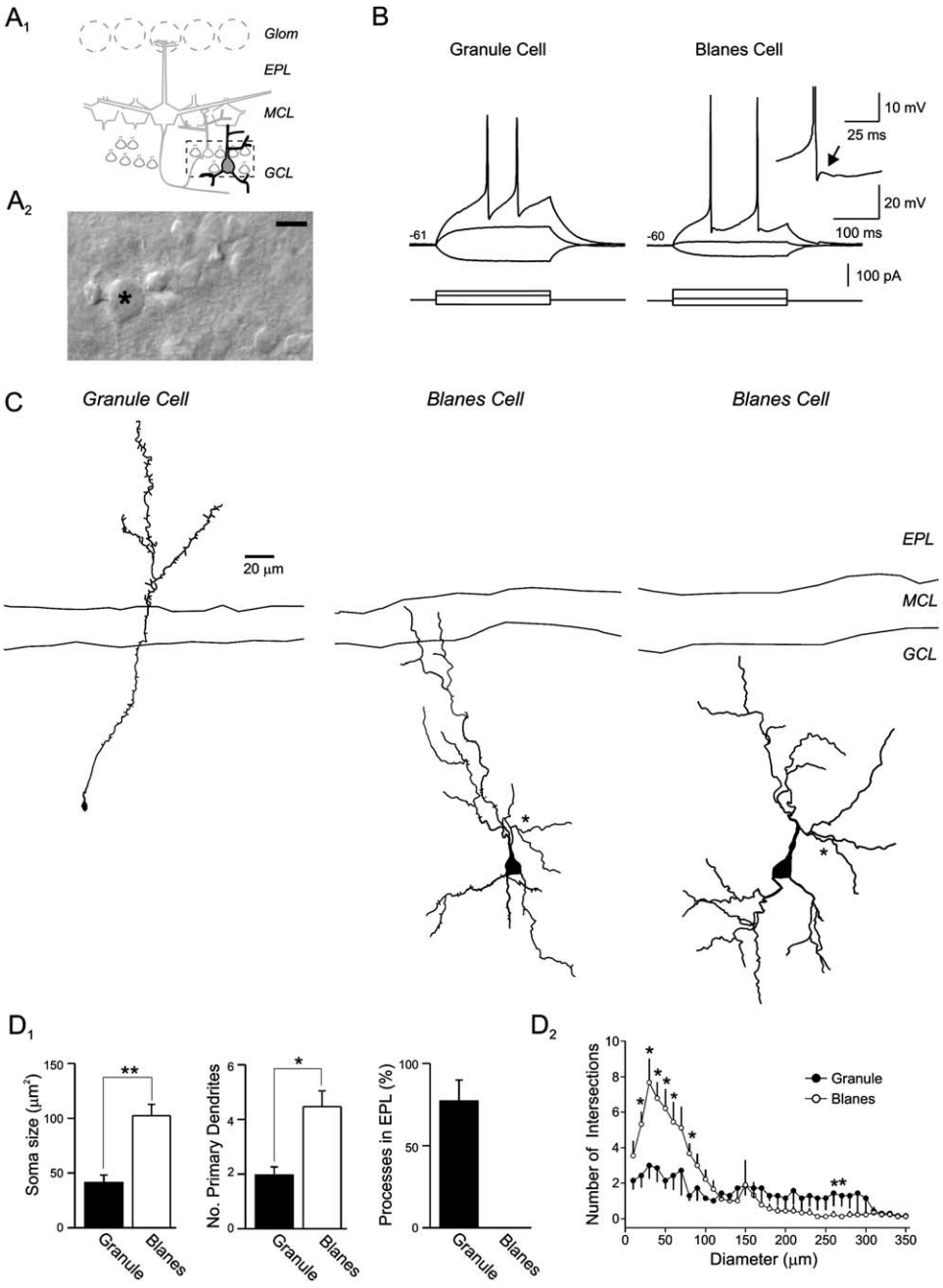

Figure 1. Multiple Cell Types in Granule Cell Layer of the Olfactory Bulb

(A_1) Schematic diagram of the olfactory bulb. Layers indicated are glomerular layer (Glom), external plexiform layer (EPL), mitral cell layer (MCL), and granule cell layer (GCL). (A_2) Infrared DIC image of the granule cell layer in a rat olfactory bulb slice. The asterisk indicates the cell body of a large non-granule Blanes neuron in the granule cell. Scale bar, 20 μm.

(B) Responses to hyperpolarizing and depolarizing current injections in granule and Blanes cells.

(C) Reconstructions of neurobiotin-labeled granule and Blanes neurons. Presumptive axons on Blanes cells are indicated by asterisks.

(D_1) Comparison of soma size, number of primary dendrites, and percentage of cells with processes that enter the external plexiform layer between granule cells and Blanes cells. We never observed a Blanes cell process enter the EPL (no bar shown in graph), whereas 86% of intracellularly stained granule cells had processes in the EPL. *$p < 0.002$, **$p < 0.001$. (D_2) Sholl analysis of dendritic branching pattern in Blanes cells (open circles) and granule cells (closed circles). *$p < 0.05$.

cells—termed Blanes neurons, reflecting their dendritic morphology (see below)—were present throughout the extent of the granule cell layer (GCL) and often were located between stripes of granule cells (Figure 1A). We used whole-cell patch-clamp recording to determine whether these large cells represent a novel cell type. Current-clamp recordings from large cells located in the granule cell layer (n = 547 cells in this study) typically showed large-amplitude overshooting action potentials (63.0 ± 1.5 mV; n = 26) and high input resistances

(260 ± 28 MΩ; n = 19), suggesting that they represent a potentially novel cell type and not a subpopulation of injured granule cells.

Large cells in the GCL differed from nearby granule cells in their intrinsic electrophysiological properties (Figure 1B). The mean input resistance of Blanes neurons was significantly lower than granule cells (260 ± 28 MΩ versus 463 ± 63 MΩ; $p < 0.001$). The mean action potential threshold in Blanes cells was also significantly more hyperpolarized than granule cells (−41.1 ± 0.8 mV, n = 26 versus −27.2 ± 1.3 mV for granule cells, n = 7; $p < 0.001$). The mean resting membrane potential in Blanes cells was more depolarized than that of granule cells (−53.9 ± 1.1 mV, n = 22 versus −65.7 ± 2.1 mV, n = 12; $p < 0.001$). Other intrinsic properties were similar in Blanes cells and granule cells, including action potential width (2.09 ± 0.09 ms, n = 26 versus 2.09 ± 0.16 ms, n = 7 granule cells) and the amplitude of the afterhyperpolarization following a single action potential (16.2 ± 0.8 mV, n = 26 large cells versus 18.1 ± 2.9 mV, n = 7 granule cells). A subpopulation of large cells (~23%) showed a pronounced depolarizing notch during the spike afterhyperpolarization (Figure 1B, inset). Other large cells showed a less prominent inflection at the same time following the spike; granule cells never displayed depolarizing notches or inflections following action potentials. Both granule cells and Blanes cells fired tonically with depolarizing current injection.

We used the Neurolucidia reconstruction system (Microbrightfield, Williston, VT) and two-photon microscopy to define the dendritic and axonal morphology of Blanes cells. Twenty-two Blanes neurons were filled with neurobiotin (0.5%; Molecular Probes) through the patch pipette and processed using the ABC peroxidase method to reveal dendritic and axonal processes. All 22 visualized Blanes neurons exhibited afterdepolarizations and persistent firing following suprathreshold 500 ms depolarizing steps, two characteristics of Blanes neurons described below. Eight visually and electrophysiologically identified granule cells also were filled with neurobiotin and processed using the ABC method. Figure 1C illustrates the dendritic morphology of one granule cell and two typical Blanes neurons. Occasionally, processes of Blanes cells entered the mitral cell layer (see middle panel in Figure 1C; 3/9 reconstructed cells); however, we never observed processes that entered the external plexiform layer (0/9 cells; Figure 1D_1). Most granule cells visualized had an apical dendritic process that ramified in the external plexiform layer and had frequent large spines associated with reciprocal dendrodendritic synapses (Rall et al., 1966). Blanes neurons, by contrast, rarely had a prominent apically directed process. Morphometric analyses revealed significant differences between Blanes and granule cell soma size (117.7 ± 11.9 μm^2 versus 47.4 ± 8.0 μm^2; $p < 0.001$) and the number of primary dendrites (4.6 ± 0.6 versus 2.0 ± 0.3; $p < 0.002$; Figure 1D_1). Blanes neurons and granule cells also differed in the extent of their dendritic aborization as quantified by Sholl analysis (Figure 1D_2). Blanes cells generated significantly more of their dendritic aborization within 100 μm of the cell body than did granule cells. While we observed small dendritic spines in neurobiotin-filled Blanes cells, these spines were not as large or numerous as the spines on the distal

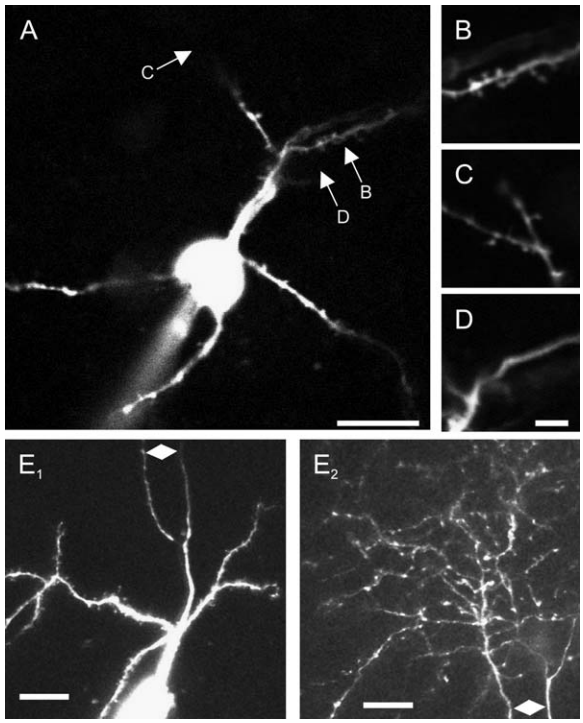

Figure 2. Visualization of Blanes Cell Morphology with Two-Photon Microscopy

(A) Two-photon image of a dendritic morphology of Blanes neuron filled with 100 μM Alexa 594 through the patch pipette. Scale bar, 20 μm.

(B and C) Enlargements of dendritic segments with dendritic spines from locations indicated on panel (A).

(D) Enlargement of presumptive axon. Scale bar on panels (B)–(D) is 5 μm.

(E_1) 2P image of soma/proximal dendrite region of a different Blanes cell filled with Alexa 594. Diamond symbol indicates presumptive main axon and axon collateral. (E_2) 2P image of axon plexus in the GCL formed by the axonal processes indicated by the diamond symbol in (E_1). The center of the axon plexus was ~250 μm away from the cell body shown in (E_1). Scale bar, 20 μm.

dendrites of granule cells. Two-photon microscopy of Alexa594-filled Blanes cells also revealed some spines on primary dendrites (Figures 2A–2C). Most Blanes neurons had a presumptive axonal process that emanated from a primary dendrite and ramified in the granule cell layer (Figures 2D and 2E). Occasionally, the axonal plexus entered the mitral cell layer; we never observed presumptive axonal processes in the external plexiform layer. Axon-like processes typically branched at right angles, did not taper, and were devoid of spines under two-photon visualization (Figure 2D).

We used paired recordings to determine the transmitter phenotype and to define the synaptic targets of Blanes cells. Because both neurobiotin visualization and two-photon fluorescence imaging revealed a presumptive axon in Blanes cells that ramified in the granule cell layer, we focused our search for potential postsynaptic targets on granule cells. We utilized two-photon imaging to determine the specific region within the GCL where the Blanes cell axon bifurcates (see Experimental Procedures). We then tested 18 Blanes/granule cell pairs using the two-photon axon visualization method. Of these paired recordings, 17% (3 of 18)

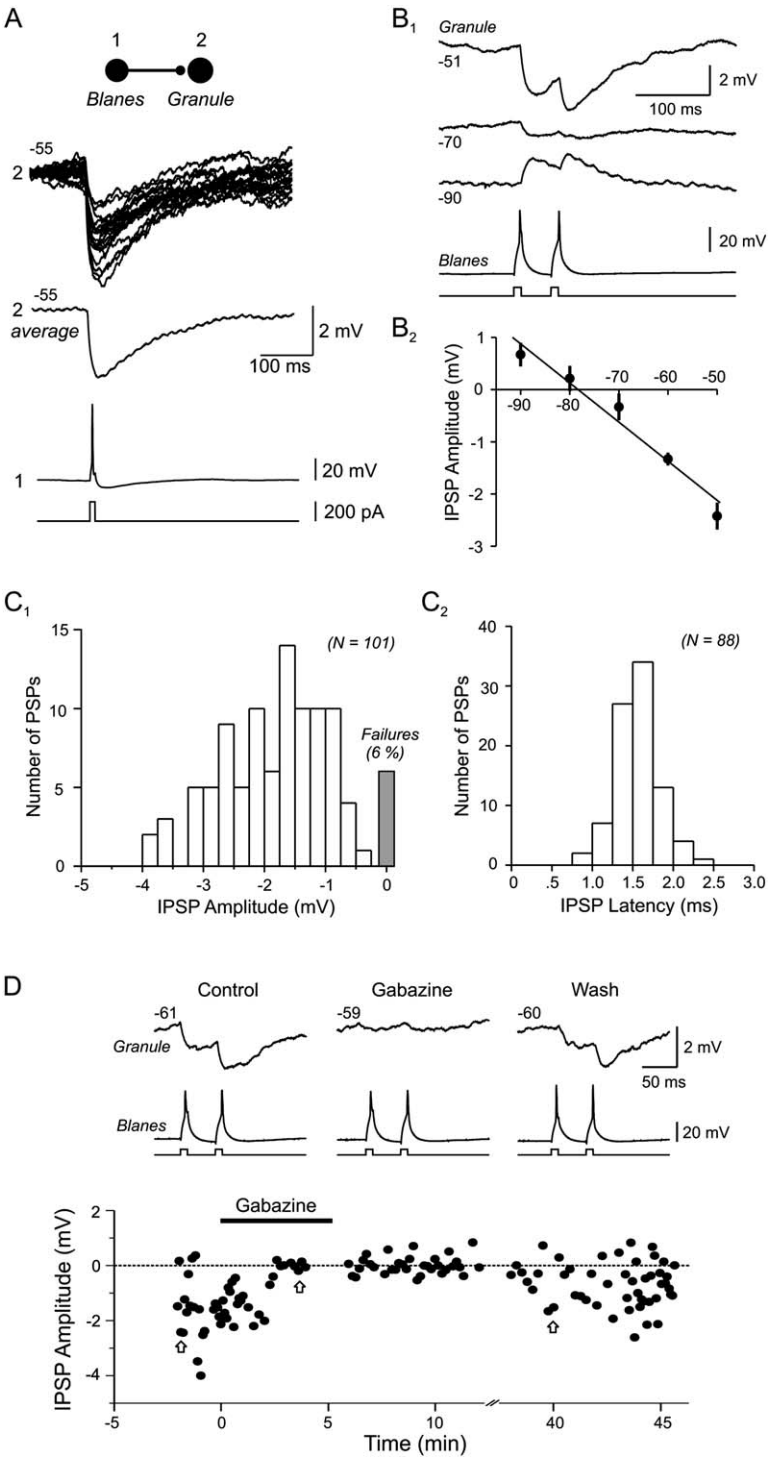

Figure 3. Blanes Cells Are GABAergic and Innervate Granule Cells

(A) Granule cell responses to 20 successive Blanes cell action potentials. Blanes cells reliably evoked hyperpolarizing IPSPs in a granule cells held at −55 mV. Average response in granule shown in middle trace.

(B_1) Blanes cell-evoked IPSPs reversed polarity near the chloride equilibrium potential. Granule cell postsynaptic responses recorded at −51 mV, −70 mV, and −90 mV; IPSPs evoked by two action potentials separated by 50 ms. (B_2) Plot of mean IPSP amplitude versus membrane potential in three Blanes-granule cell pairs (mean reversal potential = −78.3 mV).

(C_1) Amplitude distribution of Blanes cell-evoked IPSPs (mean amplitude = −1.76 ± 0.1 mV; n = 101 presynaptic action potentials, including 6 failures). (C_2) Onset latency distribution for the same Blanes/granule paired recording (mean latency = 1.54 ± 0.03 ms; n = 88).

(D) Monosynaptic Blanes cell-evoked IPSPs are reversibly blocked by the $GABA_A$ receptor antagonist gabazine (10 μM). Top traces show averages of five consecutive responses at the times indicated by the open arrows in the bottom time plot. Blanes cell-evoked IPSPs in this paired recording were not affected by NBQX (5 μM) and D-APV (50 μM; data not shown).

Responses shown in (A) and (B)–(D) were recorded from different Blanes/granule cell pairs.

generated monosynaptic IPSPs onto granule cells with onset latencies <2.5 ms. The cell bodies of the three monosynaptic pairs that we found using two-photon-guided recordings were separated by 400, 560, and 1100 μm. We found no monosynaptic pairs that generated EPSPs onto granule cells, and we never observed a reverse projection (from granule to Blanes cell). We also recorded from 83 Blanes/granule cell pairs with cell bodies separated by <80 μm using conventional IR-DIC visualization methods. Of these 83 pairs, we found one monosynaptically coupled Blanes/granule cell pair (mean onset latency = 1.81 ± 0.04 ms; n = 96 PSPs).

Figure 3A illustrates a typical Blanes-to-granule cell paired recording. In this paired recording, single Blanes cell action potentials generated short latency hyperpolarizations (mean latency = 1.51 ± 0.04; n = 20 IPSPs; Figure 3A) with a low (6%) failure rate. The mean failure rate was 7.2% ± 2.8% in our population of four paired recordings. As shown in Figure 3B, Blanes cell-evoked

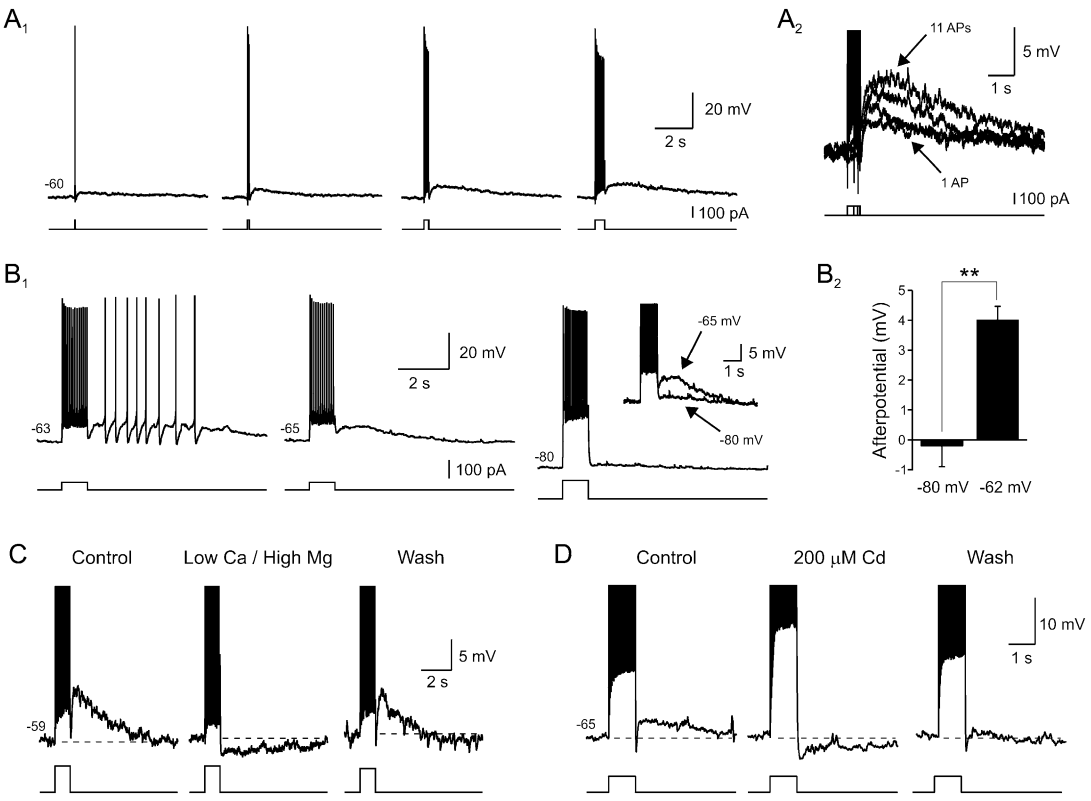

Figure 4. Afterdepolarizations in Blanes Cells

(A) Afterdepolarizations evoked by graded duration suprathreshold current steps; responses enlarged and aligned to step offset in (A_2).

(B_1) Responses to depolarizing steps at different membrane potentials. Adapting firing triggered by ADPs in Blanes cells (left panel). Afterdepolarization is voltage dependent and is not present at −80 mV. Step amplitude increased at −80 mV to trigger the same number of action potentials as at −65 mV. The inset shows superposition and enlargement of responses at −65 and −80 mV. (B_2) Summary plot of afterpotential amplitude at −80 mV and at −62 mV from six experiments. **$p < 0.001$.

(C) Decreasing Ca influx by switching to a low Ca (0.5 mM), high Mg (6 mM) external solution reversibly abolishes the ADP response. Current step = 50 pA.

(D) The ADP also is blocked by 200 μM $CdCl_2$. Current step = 200 pA.

IPSPs reversed polarity near the chloride equilibrium potential (reversal potential = −78.9 ± 0.4 mV; n = 3 postsynaptic cells), suggesting that Blanes cells make GABAergic synapses onto granule cells. The mean amplitude of the IPSP recorded in this granule cell at −55 mV was −1.8 ± 0.1 mV (Figure 3C_1; n = 101 IPSPs). The average IPSP latency in our experiments was 1.74 ± 0.15 ms (n = 4 paired recordings; range 1.46–2.13 ms) and the average amplitude at −55 mV was −1.84 ± 0.04 mV (Figure 3C_2; n = 3). We used the specific $GABA_A$ receptor antagonist gabazine (10 μM) to test this hypothesis. Gabazine reversibly blocked Blanes cell-evoked IPSPs in all three monosynaptic Blanes/granule cell paired recordings (Figure 3D). In one Blanes/granule cell pair, we also confirmed that blockers of ionotropic glutamate receptors (5 μM NBQX and 50 μM D-APV) did not affect the IPSP evoked in action potentials in the Blanes cells (data not shown). These results demonstrate that Blanes cells monosynaptically inhibit granule cells in the olfactory bulb by activating $GABA_A$ receptors.

Afterdepolarizations in Blanes Neurons

We focused our study on a subset of large neurons in the GCL, which we term "Blanes cells" based on their dendritic morphology (compare Figure 1 in Schneider and Macrides, 1978, with Figure 1C in the present study). In addition to the morphological differences discussed in the previous section, Blanes neurons and granule cells differed in their responses to short trains of action potentials. While granule cells typically responded to a burst of action potentials with a large-amplitude afterhyperpolarization (AHP), all Blanes cells visualized following intracellular staining (n = 46) generated an afterdepolarization (ADP) rather than an AHP following similar stimuli. In addition to generating ADPs, Blanes cells could fire persistently at depolarized membrane potentials (see below). Across our entire population of large neurons in the GCL recorded under current-clamp conditions, 72% (361 of 498, including the 46 cells that were intracellularly stained) generated ADPs and could fire persistently. Preliminary studies of the subpopulation of large cells that showed an AHP rather than an ADP following bursts of action potentials revealed a range of different dendritic morphologies (e.g., long horizontally or vertically oriented dendrites), suggesting that multiple interneuronal subtypes exist within the GCL (Schneider and Macrides, 1978).

Single spikes reliably triggered ADPs in Blanes cells; ADPs were graded in amplitude with additional spikes (Figure 4A). Afterdepolarizations evoked by bursts of

8 to 12 action potentials also have different kinetics than ADP responses to single spikes (Figure 4A$_2$). Afterdepolarizations were voltage dependent and were not present when the Blanes neuron was held at −80 mV (tested with increased step amplitude to trigger a similar number of action potentials evoked by steps at −60 mV; ADP amplitude significantly different between −60 and −80 mV; 4.01 ± 0.45 mV and −0.20 ± 0.69 mV, respectively; $p < 0.001$; Figure 4B). When Blanes cells were held at more depolarizing potentials (−65 to −50 mV), ADPs triggered multiple action potentials in Blanes cells. The firing frequency in the resulting train decremented during the response (see left panel on Figure 4B$_1$), suggesting that Blanes cell spiking was driven directly by the ADP. A different firing mode (discussed below) characterized by persistent, nonadapting spiking also was observed in Blanes cells following stronger stimulation.

Afterdepolarizations in Blanes cells were Ca dependent and were reversibly blocked by a low Ca (0.5 mM), high Mg (6 mM) external solution (ADP reduced to 3.1% of control; n = 4; $p < 0.02$; Figure 4C). We used the inorganic channel blocker Cd to determine whether Ca influx through voltage-dependent Ca channels (VDCCs) is required to trigger an ADP. In all five Blanes cells tested, 200 μM Cd blocked the ADP (ADP reduced to −27.7% ± 11.6% of control; n = 4; $p < 0.001$; Figure 4D) and revealed a residual afterhyperpolarization. The ADP was unaffected by the L-type VDCC blockers nifedipine (50 μM; 89.4% ± 4.6% of control; n = 5 cells) and nitrendipine (20 μM; 90.0% ± 7.0% of control; n = 5 cells). The ADP also was unaffected by the L-type VDCC modulator S-(-)-Bay K 8644 (1 μM; 96.0 ± 7.0; n = 5 cells). We then used EGTA to determine whether the ADP resulted from an intracellular signaling action of Ca or instead reflected an inward current mediated by voltage-dependent Ca channels. Five Blanes cells were recorded using pipettes whose tips contained low EGTA solution (0.2 mM) and were backfilled with the same internal solution supplemented with 10 mM EGTA. In all five cells, depolarizing steps evoked ADPs immediately after break-through into the whole-cell recording mode. These responses gradually declined over 30–40 min until they reached steady-state levels (at 5.9% ± 17% of control; Figure 5A). The ADP response showed only a modest decay (to 83% ± 9% of control amplitude; n = 3 cells) over a similar recording period (mean 40 min) in interleaved control experiments using electrodes backfilled with the low EGTA internal solution. The ADP amplitude in high EGTA experiments was significantly reduced compared with control experiments using 0.2 mM EGTA at 40 min ($p < 0.01$; summarized in inset in Figure 5A). These results suggest that the ADP was due to an EGTA-sensitive Ca signaling pathway activated by Ca entry through a non-L-type VDCCs.

Next, we used the photolyzable Ca chelator NP-EGTA (Ellis-Davies and Kaplin, 1994; Hall and Delaney, 2002) to test whether a transient increase in intracellular Ca is sufficient to trigger an afterdepolarization in Blanes cells. In a majority of the neurons with large cell bodies recorded in the granule cell body layer (18 of 34), brief exposure to UV illumination (400–2000 ms) evoked an inward current when the cell was voltage clamped near rest (−60 to −80 mV). In a minority of large cells, UV exposure evoked an outward current (10 of 34 cells) or no

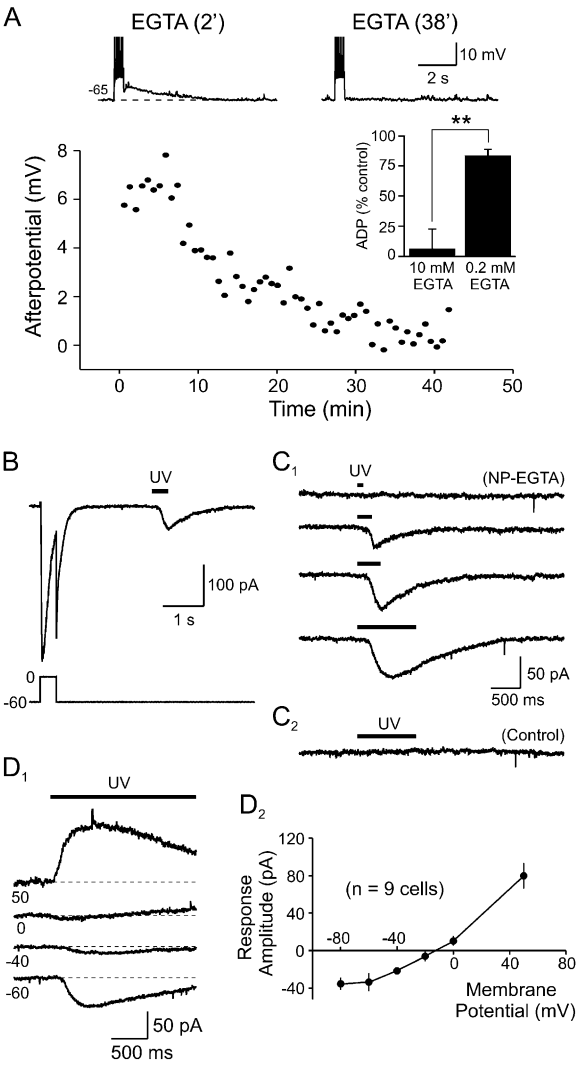

Figure 5. Calcium-Dependent Afterdepolarizations in Blanes Cells

(A) Afterdepolarization is abolished by the intracellular Ca chelator EGTA. Responses shown 2 min following breakthrough to whole-cell recording mode (six APs) and after 38 min (seven APs). Pipette tip filled with low EGTA (0.2 mM) intracellular solution; high EGTA (10 mM) solution used to backfill pipettes. Lower graph shows reduction in ADP amplitude during recording. The inset shows summary graph of percent ADP reduction with high EGTA backfill experiments (n = 4) and with interleaved control experiments (backfilled with 0.2 mM EGTA; n = 3). Current step = 200 pA. **$p < 0.01$.

(B) Photolyzing NP-EGTA (2 mM) evokes an inward current in Blanes cells voltage clamped at −60 mV. The UV illumination timing is indicated by the horizontal bar above the trace. Blanes cells were transiently depolarized to 0 mV 2–3 s before each period of UV illumination to maximize the concentration of Ca bound to NP-EGTA. (Uncaging responses shown in subsequent traces begin after this step depolarization.)

(C_1) Responses to a series of graded duration UV exposures (100, 250, 400, 1000 ms long). (C_2) A 1 s duration UV exposure fails to elicit a response in a Blanes cell filled with a control internal solution without any added NP-EGTA.

(D_1) Responses to UV exposure in Blanes cells loaded with NP-EGTA reverse polarity near 0 mV. (D_2) Summary plot of the peak amplitude of the responses to UV exposure at different holding potentials in nine voltage-clamped Blanes cells.

response (6 of 34 cells), suggesting that there may be multiple subtypes of large neurons in the granule cell layer. The mean amplitude of the response to a 2 s photolysis of NP-EGTA at −40 mV was −16.2 ± 2.8 pA (n = 12 cells with inward currents). As shown in Figure 5C_1, varying the duration of light exposure from 100 to 1000 ms generated a graded series of inward currents. Two second light exposures to a Blanes cell recorded with a control internal solution that did not contain NP-EGTA failed to generate a response (n = 5 cells; Figure 5C_2). The light-activated inward current was associated with a 68.0% ± 7.0% decrease in input resistance measured using small depolarizing test pulses applied during maximal inward current (10 mV, 100 ms duration; n = 5 cells; p < 0.01; data not shown). The light-activated response reversed polarity at −10.7 ± 5.8 mV (n = 9 cells; Figure 5D_1) and had a modest voltage dependency (Figure 5D_2), consistent with the properties described previously for the Ca-activated nonselective cation current (I_{CAN}) in other cell types (Haj-Dahmane and Andrade, 1998, 1999; Hall and Delaney, 2002).

Our results thus far suggest that a Ca-dependent response underlies the afterdepolarization in Blanes cells. We next sought to determine whether this response reflects the activation of a Ca-dependent inward current (e.g., I_{CAN}) or is mediated by a transient decrease in a resting K current. Depolarizing responses mediated by transient reductions in K currents are highly sensitive to changes in extracellular K concentration (Li and Hatton, 1997). As shown in Figure 6A, doubling the extracellular K concentration (from 3 to 6 mM) did not affect the amplitude or time course of the ADP response in Blanes cells (98.4% ± 2.9% of control; n = 5; tested after adjusting the DC current to return the neuron to the original resting membrane potential), suggesting that the ADP is not mediated by a decrease in K currents. Increasing extracellular K concentration did reduce the fast afterpolarization that immediately follows the step offset (Figure 6A, arrow), suggesting that multiple responses probably shape the afterdepolarization responses in Blanes cells. We also found that the specific M-current blocker XE-991 (30 μM) depolarized Blanes cells but did not affect the burst-evoked ADP (101.2% ± 9.9% of control; n = 8; data not shown). Calcium spikes evoked in the combination of TTX (1 μM), TEA (25 mM), and 4-AP (100 μM) also triggered ADPs (Figure 6B, middle trace), which displayed the same voltage dependence as ADPs evoked under control conditions (n = 12). These results suggest that the ADP was not mediated by a decrease in standing outward currents. In contrast with the results obtained by altering [K], reducing extracellular Na ions by partially substituting with the impermanent ion NMG (99 mM) strongly attenuated ADPs triggered by Ca spikes in Blanes cells (9.7% ± 14.5% of control; n = 7; p < 0.001; Figure 6B). The reduction in ADPs in low Na ACSF was fully reversible upon washout of the NMG solution (data not shown). Low Na ACSF also increased the amplitude of the fast AHP that immediately followed the step offset, suggesting that ADP and this hyperpolarizing response overlap.

Nonselective cation currents often mediate spike- and burst-evoked afterdepolarizations in neurons in other brain areas (Egorov et al., 2002; Haj-Dahmane and Andrade, 1998; Hall and Delaney, 2002; Partridge et al., 1994). We used flufenamic acid (FFA), a partially selective I_{CAN} blocker (Ghamari-Langroudi and Bourque, 2002; Partridge and Valenzuela, 2000), to test whether Blanes neuron ADPs are mediated by I_{CAN}. Because preliminary experiments demonstrated a nonspecific action of FFA on fast Na currents, we tested FFA on ADPs evoked by short trains of Ca spikes in TTX, 4-AP, and TEA. Under these conditions we found that 200 μM FFA significantly reduced the ADP amplitude (to 31.0% ± 13.5% of control; n = 7; p < 0.002; Figures 6C and 6D). As shown in Figure 6C, this action was fully reversible upon washout of FFA. Flufenamic acid decreased the number of Ca spikes evoked by the current step. However, afterdepolarization amplitude was still significantly reduced by FFA (to 61.6% ± 6.3% of control; n = 7; p < 0.001) even after we controlled for this action by increasing the current step amplitude to trigger the same number of Ca spikes (Figure 6C). Together, these data point to I_{CAN} as the underlying mechanism responsible for ADPs in Blanes cells. However, the absence of selective I_{CAN} antagonists or applicable molecular tools precludes definitively ruling out other potential Ca-sensitive mechanisms for the ADP.

Persistent Spiking in Blanes Neurons

In addition to evoking Ca-dependent afterdepolarizations, depolarizing current steps also triggered prolonged periods of tonic firing in Blanes neurons held near firing threshold. The transition between afterdepolarization, which could trigger several irregularly spaced action potentials, and persistent firing was governed by both membrane potential (Figure 7A) and stimulus amplitude (Figure 7B_1). Near spike threshold, the duration of the ADP-triggered spike train was highly sensitive to membrane potential and increased as the cell was held closer to firing threshold (Figure 7A). Depolarizing stimuli that reliably triggered persistent firing in Blanes cells failed to elicit prolonged firing in granule cells and instead evoked afterhyperpolarizations (Figure 7B_2; n = 53 cells). The frequency of persistent firing in a Blanes cell was relatively invariant and not affected by changes in the step amplitude (Figure 7C_1). While we occasionally observed persistent firing triggered by single action potentials, in most cells a 100–500 ms duration suprathreshold depolarizing step was required to trigger persistent firing. The frequency of persistent firing varied considerably among Blanes neurons (Figure 7C_2; mean firing frequency = 6.5 Hz; range 3.1–13.4 Hz; n = 61 cells). However, the frequency of tonic firing was relatively constant with repeated trials in the same cell (CV = 0.10 ± .01; n = 13 cells). Persistent firing also could be triggered by uncaging Ca in Blanes cells loaded with NP-EGTA (2 mM; Figure 7D). Exposure to UV light alone did not depolarize Blanes cells or initiate persistent firing in control experiments without NP-EGTA added to the internal solution (n = 3 cells; Figure 7D, bottom trace). As shown in Figure 7E, persistent firing in Blanes cells evoked periodic IPSPs in monosynaptically coupled granule cells (mean IPSP latency to single spikes = 1.54 ± 0.03 ms; mean IPSP latency following individual spikes during persistent firing = 1.47 ± 0.05 ms).

Persistent firing was reversibly abolished in low Ca/high Mg ACSF (Figure 8A; n = 4) and was unaffected by the L-type voltage-dependent Ca channel blocker

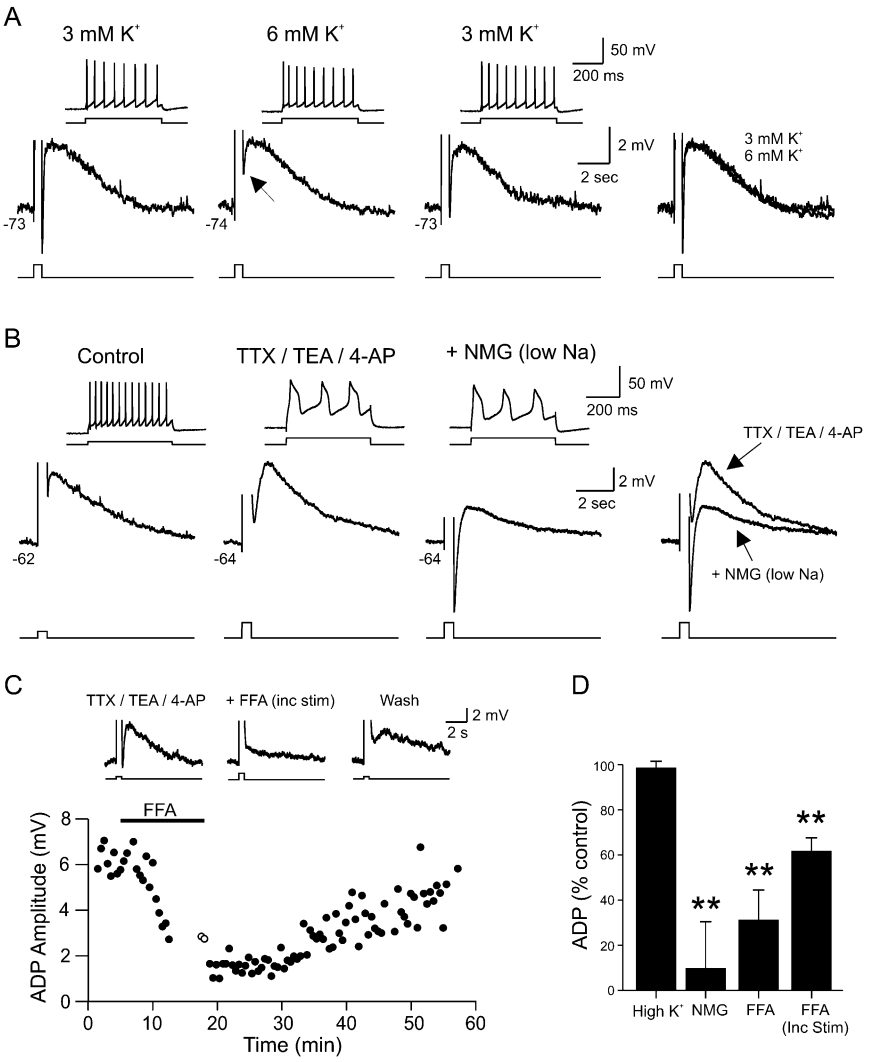

Figure 6. Afterdepolarizations Are Blocked by I_{CAN} Antagonists

(A) Increasing extracellular [K] concentration from 3 to 6 mM does not affect afterdepolarization. Superimposed responses recorded in 3 and 6 mM [K] shown in right panel. Elevated [K] did reduce the amplitude of the fast afterhyperpolarization immediately following the step depolarization (arrow in middle trace). Responses to the step depolarizations are shown in inserts above each trace.

(B) Afterdepolarizations were evoked by a train of Ca spiked after Na and K channels were blocked using bath application of TTX (1 μM), TEA (25 mM), and 4-AP (100 μM). The amplitude of the ADP evoked by Ca spikes was reduced in low Na ACSF. Responses before and after switching to low Na ACSF are superimposed on the right panel.

(C) Plot of the reduction in ADP amplitude by the I_{CAN} blocker FFA (200 μM). In most cells, FFA decreased the number of Ca spikes triggered by the depolarizing steps. We increased the amplitude of the depolarizing step in several episodes (open circles) so as to trigger the same number of Ca spikes as in control. Traces above plot show control ADP, response in FFA to a larger amplitude step [+ *FFA (inc stim)*], and following washout of FFA.

(D) Summary of experiments with elevated [K], NMG substitution, and FFA. **$p < 0.002$.

nifedipine (50 μM; n = 5; data not shown). These results suggest that non-L-type voltage-dependent Ca channels contribute to the initiation or maintenance of persistent firing. The ability of low Ca ACSF to block persistent firing was not likely due to blockade of synaptic transmission, as persistent firing was unaffected by antagonists of iontropic glutamate (5 μM NBQX and 25 μM D-APV; n = 28) or $GABA_A$ receptors (10 μM gabazine or 50 μM picrotoxin; n = 4).

Once triggered, persistent firing typically persisted for many minutes before spontaneously returning to the pre-step membrane potential. The average duration of tonic firing was 16.5 ± 5.1 min (range 1.5–44.1 min; n = 9). As shown in Figure 8B_1, tonic firing did not stop abruptly but rather gradually decreased over 1–2 min. This gradual decrease in average firing rate was due in part to increasingly frequent pauses between runs of spikes at the original firing frequency. Enlargements of these pauses often revealed small depolarizing peaks (Figure 8B_2). The intervals between the preceding action potential and these depolarizing peaks were similar to the intervals between successive action potentials during the initial tonic firing phase, suggesting that tonic firing frequency may be governed by the kinetics of the spike afterpolarization. We recorded persistent firing lasting at least 10 s in the majority of Blanes cells tested

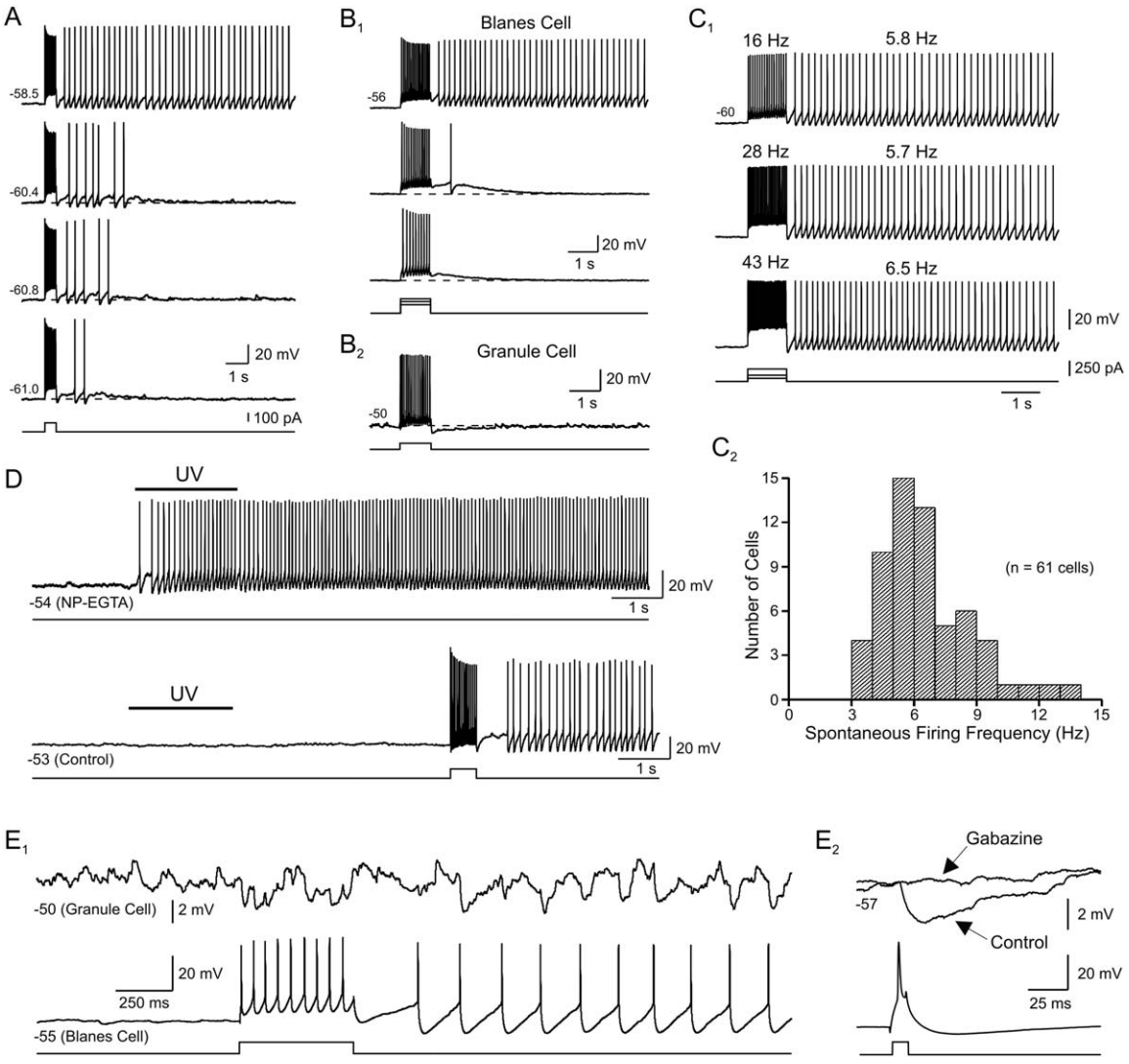

Figure 7. Brief Depolarizations Trigger Persistent Firing in Blanes Cells

(A) Responses to constant step depolarizations at different membrane potentials (indicated above trace). Persistent firing evoked at the most depolarized membrane potential (−58.5 mV).

(B_1) Transient and persistent firing modes evoked at the same membrane potential by graded depolarizing steps (60, 80, 100 pA). (B_2) Similar depolarizing current steps (100 pA) evoked an afterhyperpolarization in granule cells.

(C_1) Frequency of persistent firing was not affected by modulating the amplitude of the initiating depolarizing step. (C_2) Distribution of the frequencies of persistent firing in 61 Blanes cells activated by step depolarization. The mean firing frequency in this population of Blanes cells was 6.5 Hz.

(D) Persistent firing evoked by uncaging Ca. Light exposure (*UV*, duration indicated by bar above trace) in a Blanes cells recorded with NP-EGTA (2 mM) in the internal solution depolarized the neuron and initiated tonic firing. No response was observed to light exposure in a control experiment (below) in which NP-EGTA was not added to the internal solution. Persistent firing was induced by a depolarizing step in this cell near the end of the record.

(E_1) Paired recording between a Blanes cell (bottom trace) and a monosynaptically coupled granule cell held at −50 mV (top trace). Single Blanes cell action potentials consistently evoked a short-latency (1.54 ± 0.03 ms; same paired recording as in Figure 3C) IPSP in this granule cell. A 500 ms long depolarizing step to the Blanes cell evoked a barrage of IPSPs in the granule and triggered persistent firing in the Blanes cell. The resulting persistent firing at 5.9 Hz in the Blanes cell triggered persistent inhibition in the granule cell. (E_2) Gabazine (10 μM) blocked spike-evoked IPSPs in this Blanes-granule cell paired recording.

systematically (58 of 79 cells). Persistent firing could generally be triggered when the membrane potential was within 10–15 mV (mean 11.8 mV; n = 23 cells) below the action potential threshold. Most Blanes cells we recorded had resting membrane potentials that were within this window (mean RMP = −53.9 ± 1.1 mV; mean AP threshold = −41.1 ± 0.8 mV).

Persistent firing was not affected by brief hyperpolarizing current injections that temporarily blocked spiking (Figure 8C; firing maintained in 10 of 10 cells after 1 s duration hyperpolarizing pulses with a mean amplitude of −24 mV; firing maintained in 5 of 6 cells after 3–6 s duration pulses with a mean amplitude of −43 mV) but was blocked by a prolonged period (60 s) of membrane

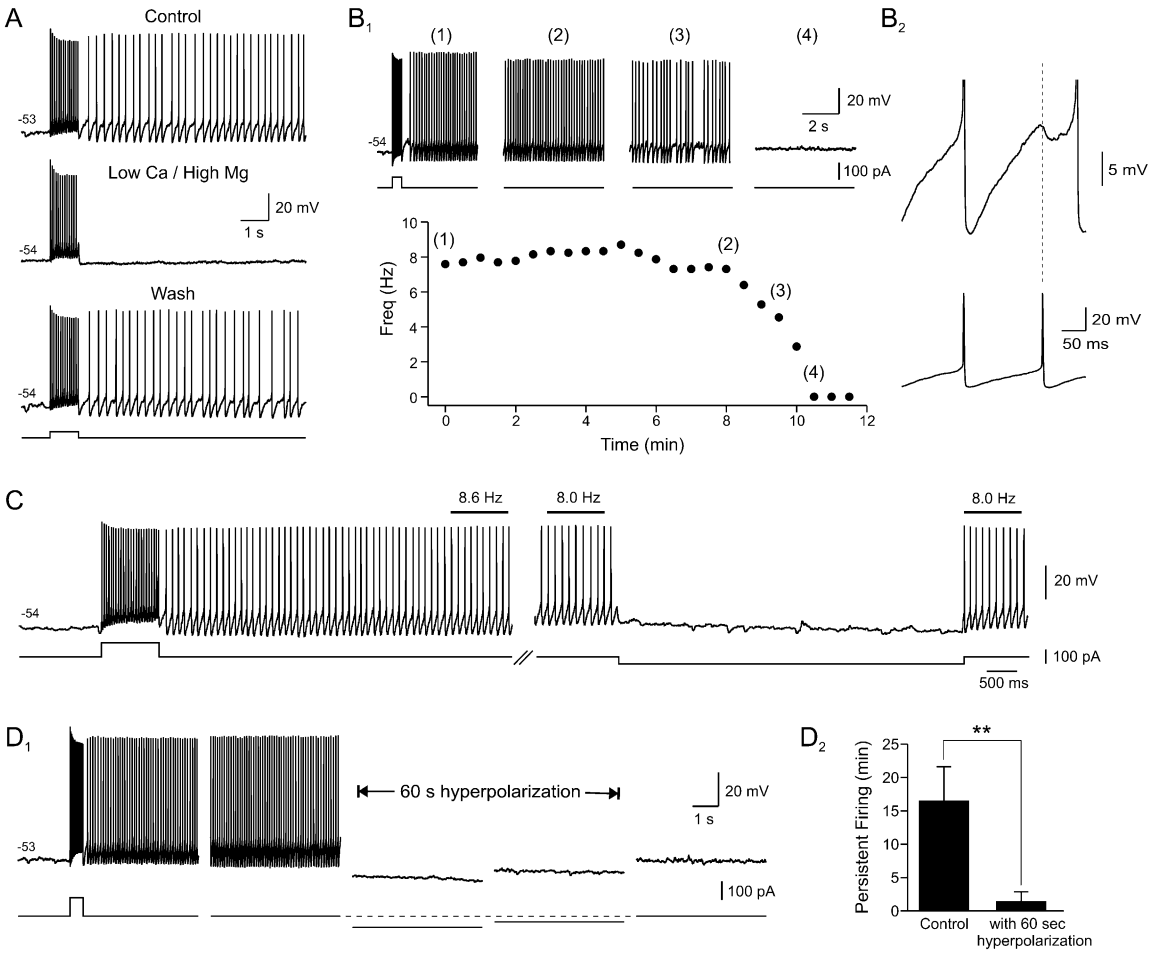

Figure 8. Prolonged Hyperpolarization Stops Persistent Firing

(A) Persistent firing is reversibly blocked by switching to a low Ca (0.5 mM), high Mg (6 mM) external solution. Current step = 50 pA.

(B_1) Plot of time course of persistent firing evoked by a 500 ms depolarizing step. Example traces from time points indicated on plot. (B_2) Enlargements of steady-state period of persistent firing (bottom trace) and the firing pattern immediately before persistent firing ceased (top trace). Cessation of persistent firing was associated with increased interspike intervals that revealed spike-evoked ADPs at the time of the expected spike.

(C) Persistent firing evoked by a 1 s depolarizing step is unaffected by transient 3 s hyperpolarization. Average firing rate indicated above trace segments indicated by solid lines.

(D_1) Persistent firing in another Blanes cell is abolished by prolonged hyerpolarization (60 s). (D_2) Summary of effect of prolonged (45–60 s) hyperpolarization on mean duration of persistent firing on ten Blanes cells. Prolonged hyperpolarization significantly reduced the average firing duration compared with interleaved control experiments (n = 9 cells) without tonic hyperpolarizing current applied. **$p < 0.005$.

potential hyperpolarization (Figure 8D; persistent firing abolished in 9 of 10 trials). The average duration of persistent firing following a 60 s hyperpolarization was significantly reduced compared with interleaved control trials without hyperpolarizing current injection (Figure 8D_2; firing duration = 1.43 min with hyperpolarization versus 16.5 min in control trials; n = 10 and 9, respectively; $p < 0.005$). Additional experiments will be needed to understand why prolonged periods of moderate hyperpolarization were more effective at blocking persistent activity than brief, large-amplitude hyperpolarizing steps.

Excitatory synaptic input to Blanes cells was an effective trigger for persistent firing. Blanes cells receive excitatory input that can be activated by extracellular stimulation in the granule cell layer (Figure 9A_2; 11 of 11 cells tested) or glomerular layer (9A_4; 10 of 10 cells tested). The average amplitude of the GCL-evoked EPSP in Blanes cells recorded at −80 mV was 4.2 ± 0.6 mV in control conditions and 0.1 ± 0.2 mV in 25 μM D-APV and 5 μM NBQX (EPSP amplitude significantly reduced; $p < 0.001$; n = 4 cells). The mean EPSP onset latency was short (1.70 ± 0.06 ms; n = 4 cells) following the GCL shock, suggesting that Blanes cells were monosynaptically excited by this stimulus. Trains of GCL layer stimuli generated summated EPSPs (see lower panel in Figure 9A_2) that reliably triggered persistent firing in Blanes cells recorded in both cell-attached (mean firing frequency = 6.3 ± 1.1 Hz; n = 7) and whole-cell modes (6.7 ± 2.1 Hz; n = 4 cells; Figure 9A_3). Single shocks to the glomerular layer often triggered prolonged EPSPs in Blanes cells that also could trigger persistent firing when the membrane potential was near firing threshold (Figure 9A_4; 6 of 6 cells tested). These data suggest that glutamatergic synaptic inputs can effectively trigger persistent firing in Blanes cells.

The same extracellular stimulation protocols that reliably triggered persistent firing in Blanes cells also triggered prolonged barrages of inhibitory postsynaptic

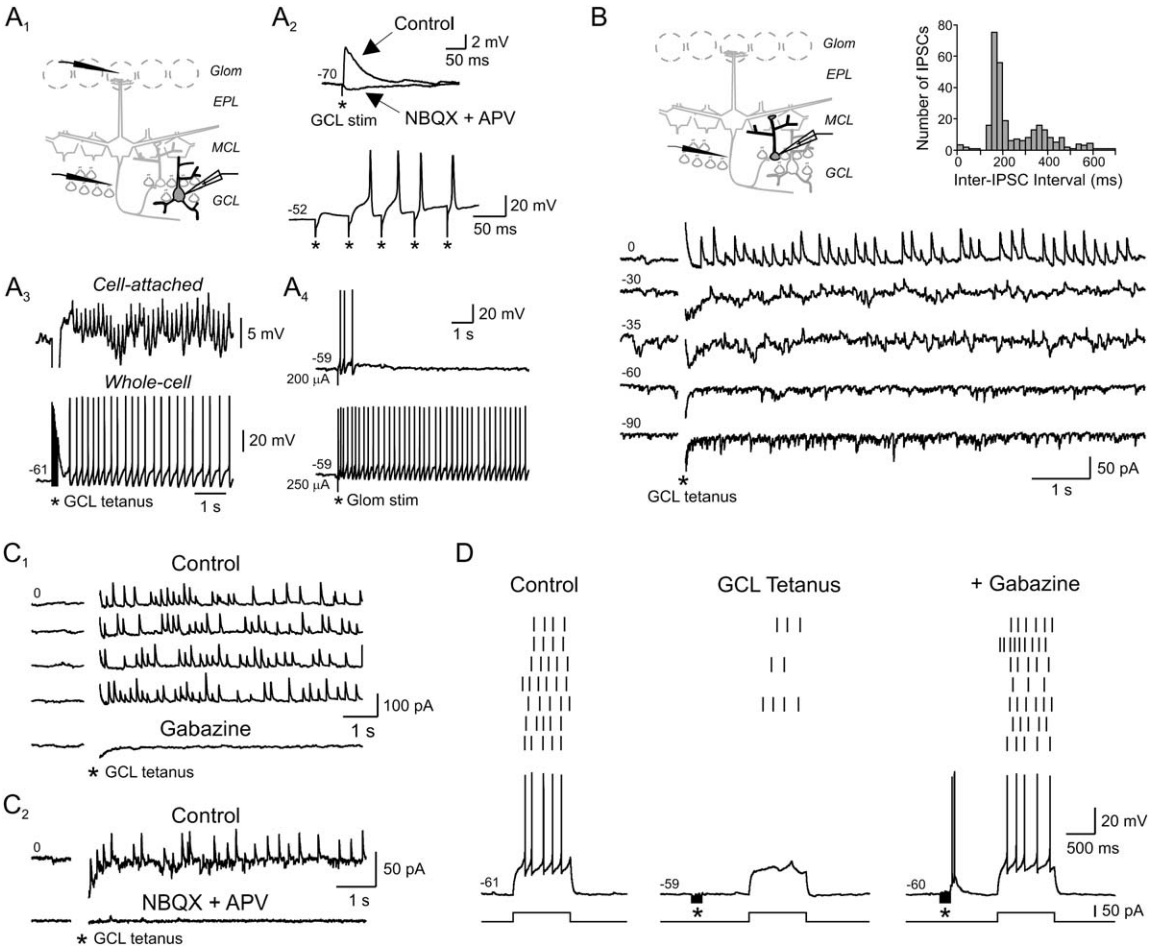

Figure 9. Synaptic Stimulation Activates Blanes Cells and Evokes Long-Lasting Inhibition onto Granule Cells

(A_1) Schematic drawing of stimulation experiment with stimulus electrodes placed in either the glomerulus layer or the granule cell layer. (A_2) Excitatory synaptic response to a single shock in the GCL was blocked by NBQX (5 μM) and D-APV (25 μM). Lower panel shows response to a train of GCL stimuli at 20 Hz. The second and subsequent GCL-evoked EPSPs triggered action potentials. (A_3) Persistent firing evoked by tetanic stimulation in the granule cell layer (ten shocks at 50 Hz). Responses recorded in both cell-attached (top) and whole-cell configuration (bottom) from the same Blanes cell. (A_4) Single shocks in the glomerular layer triggered prolonged EPSPs in Blanes cells (top) that could evoke persistent firing at increased stimulus intensity (bottom).

(B) Tetanic stimulation in the GCL evokes periodic large-amplitude IPSCs recorded in voltage-clamped granule cells held near the EPSC reversal potential (~0 mV). Both periodic IPSCs and spontaneous EPSCs were recorded at hyperpolarized membrane potentials (−30 to −90 mV). Episodes acquired at 2 min intervals. The inset shows inter-IPSC interval histogram compiled from 281 events detected in the same Blanes cell. GCL-evoked inhibitory barrages were periodic with a preferred interval of 173 ms (5.8 Hz) with a smaller second peak at the second harmonic (358 ms).

(C_1) Responses to four consecutive GCL tetani in a granule cells held at 0 mV. Periodic IPSCs evoked by this stimulus were blocked by the $GABA_A$ receptor antagonist gabazine (10 μM; bottom trace). (C_2) Persistent inhibition in granule cells evoked by a GCL tetanus also was blocked by NBQX (5 μM) and D-APV (25 μM).

(D) GCL tetani inhibited granule cell responses to test depolarizing stimuli (40 pA depolarizing step, 1 s duration). This form of functional inhibition onto granule cells was blocked by gabazine (10 μM), suggesting that is was mediated by persistent firing in inhibitory neurons. The rastergram above the traces represents the timing of step-evoked action potentials in seven consecutive trials. No spikes were triggered by the depolarizing step on 4/7 trials following the GCL tetanus. The GCL stimulating electrode was placed at least 200 μm away from the cell body in all experiments.

responses in granule cells. Figure 9B illustrates persistent IPSCs recorded in voltage-clamped granule cells held at 0 mV to minimize the amplitude of spontaneous EPSCs. Granule cell layer stimulation (ten shocks at 50 Hz; 100 μA) evoked periodic IPSCs in granule cells (Figure 9B, insert; IPSC frequency = 6.2 Hz) and approximately the same frequency that Blanes cells discharge following similar extracellular stimuli. Periodic IPSCs evoked by GCL stimulation were abolished by both the $GABA_A$ receptor antagonist gabazine (Figure $9C_1$; 10 μM) and by ionotropic glutamate receptor antagonists (Figure $9C_2$; 5 μM NBQX + 50 μM D-APV). The variation in IPSC amplitude and occasional missed oscillation cycles (Figures 9B and 9C) are consistent with the quantal nature of these synaptic responses. Based on their similar periodic nature, it is likely that these inhibitory barrages in granule cells resulted from persistent activity in one or a small number of Blanes cells. Finally, we tested whether persistent synaptic activity had functional effects on granule cells. In 4 of 4 granule cells tested in which GCL stimulation evoked inhibitory barrages, the number of action potentials evoked by test

current steps was significantly decreased when the step was preceded by a GCL tetanus (to 54.1% ± 11.1% of control; the reduction in number of spikes was statistically significant; $p < 0.02$; Figure 9D). This reduction in excitability was reversed by gabazine (4 of 4 cells), suggesting that this functional inhibition of granule cells was due to persistent inhibitory input to granule cells.

Discussion

In this study, we report for the first time the electrophysiological properties of Blanes cells, large stellate-shaped interneurons in the granule cell layer of the mammalian olfactory bulb. We used paired recordings to show that Blanes cells use GABA as a neurotransmitter and inhibit granule cells. Unlike granule cells, which have pronounced afterhyperpolarizations following repetitive spiking, Blanes cells generate depolarizing afterpotentials that allow them to continue firing following a depolarizing stimulus. When held near their action potential threshold, transient stimuli can trigger persistent spiking in Blanes cells that can be reset by hyperpolarizing current steps. Persistent activity in these feedforward GABAergic interneurons modulates tonic inhibition on granule cells and therefore is positioned to disynaptically regulate mitral and tufted cell activity.

Heterogeneous Interneuronal Subtypes in the Olfactory Bulb

A large variety of interneuronal subtypes has been demonstrated in the mammalian olfactory bulb using Golgi and immunocytochemical staining methods. On the basis of morphology, at least seven non-granule cell types have been described in the granule cell layer (Golgi cells, vertical cells of Cajal, stellate cells, short axon cells, horizontal cells, bitufted neurons, and Blanes cells; Alonso et al., 2001; Kakuta et al., 1998; Lopez-Mascaraque et al., 1986; Schneider and Macrides, 1978). However this classification system has not been adopted widely, and some authors have used both "short axon cells" and "stellate cells" to represent non-granule cells located in the granule cell layer. Many of the non-granule cells in the granule cell layer are immunoreactive for GABA or GAD, two markers for GABAergic neurons (Gracia-Llanes et al., 2003; Ohm et al., 1990), although it is not clear whether all seven non-granule cell types identified thus far are GABAergic. Similarly, many cell types located in the granule cell layer express one or more calcium binding proteins (Alonso et al., 2001; Kakuta et al., 1998), though presently there is no clear correlation between neuronal subtype and the presence of a particular protein marker. Also complicating the anatomical segregation of granule cell layer interneurons is the observation that granule cells themselves express a variety of GABAergic markers and calcium binding proteins (Alonso et al., 2001).

The major morphological features of the cell type we describe in this report (large multipolar neurons with stellate-like dendritic morphology) resemble three previously described granule cell layer neurons: Golgi cells, stellate cells, and Blanes cells. Of these three, the closest match for our cells appears to be Blanes cells (Blanes, 1898; Kakuta et al., 1998; Nakajima et al., 1996; Schneider and Macrides, 1978; Scott et al., 1987), based on dendritic morphology and the presence of dendritic spines (see Figure 1 in Schneider and Macrides, 1978). Stellate cells are similar in size to Blanes cells but are typically described in the deep part of the granule cell layer and may correspond to a subpopulation of VIP-immunoreactive interneurons (Nakajima et al., 1996). Golgi cells lack dendritic spines and also are typically reported in the deep granule cell layer (Kakuta et al., 1998; Price and Powell, 1970a; Schneider and Macrides, 1978). While our population of spiny non-granule interneurons appears relatively homogeneous in terms of intrinsic properties and persistent firing modes, we have also recorded from other large neurons in the granule cell layer that are distinct from Blanes cells. When intracellularly stained, many of these interneurons correspond to either vertical cells of Cajal or horizontal cells (Alonso et al., 2001; Kakuta et al., 1998; Schneider and Macrides, 1978). Our preliminary results suggest that most large non-granule cells in the GCL, including Blanes cells, receive fewer spontaneous synaptic inputs than granule cells. However, we also observed apparent differences in the rates and kinetics of spontaneous inputs among these cells, suggesting that defining the complex pattern of synaptic innervation to these cells will require further study.

Our results provide multiple lines of evidence that suggest that Blanes cells monosynaptically innervate granule cells. Experiments using paired recordings demonstrate that single action potentials in Blanes cells are associated with short-latency IPSPs in granule cells that are blocked by $GABA_A$ receptor antagonists. The short onset latency (mean 1.7 ms) along with the high reliability (>92% average success rate), low latency jitter, and insensitivity to glutamate receptor antagonists are all consistent with activation of a monosynaptic inhibitory pathway and are inconsistent with disynaptic inhibition. The ability to identify monosynaptically coupled Blanes/granule cell pairs using two-photon microscopy raises the possibility of visualizing the location of this synaptic connection on the granule cell dendrite in future studies. Additional ultrastructural experiments then will be necessary to define the morphological properties of the putative synaptic contacts identified using multiphoton microscopy (e.g., number of active zones, number of synapses per postsynaptic cell, number of postsynaptic neurons per Blanes cell).

Cellular Mechanism of Afterdepolarization and Persistent Firing

One of the most obvious electrophysiological differences between Blanes cells and granule cells is the large afterdepolarization evoked by suprathreshold activity in Blanes cells. This response does not appear to be mediated by polysynaptic activity, as the ADP is present after Na-based action potentials are blocked with TTX and is resistant to glutamate receptor antagonists.

The sensitivity of the ADP to the blockade of Ca influx (with either low Ca ACSF or Cd) and to intracellular perfusion with the Ca chelator EGTA suggests that it is triggered by a rise in intracellular Ca. Two potential explanations have been proposed for Ca-dependent depolarizing afterpotentials in other cell types: a transient reduction in standing outward K current (Li and Hatton, 1997; Roper et al., 2003, 2004) and Ca-activated

nonselective cation currents (Bourque, 1986; Ghamari-Langroudi and Bourque, 2002; Haj-Dahmane and Andrade, 1998; Partridge et al., 1994). We found no compelling evidence for transient reductions in standing K currents following depolarizing steps in Blanes cells. The ADP response was unaffected by blockers of H-, D-, and M-type currents; ADPs also could be evoked in slices bathed in high concentrations of TEA, which would be expected to block delayed rectifier K currents. The ADP was unaffected by raising the extracellular K concentration from 3 to 6 mM, which should passively decrease ADP responses mediated by transient decreases in standing K currents.

Several independent lines of evidence suggest that the ADP response in Blanes cells is mediated by I_{CAN}. The reversible blockade of the ADP by FFA is consistent with an I_{CAN} mechanism (Ghamari-Langroudi and Bourque, 2002; Partridge and Valenzuela, 2000), as is the reduction in ADP amplitude in low Na ACSF and the voltage dependence we observe to the ADP response (Haj-Dahmane and Andrade, 1998, 1999; Bourque, 1986). However, FFA appears to have other effects in olfactory bulb slices (e.g., it reduced the number of Ca spikes evoked by depolarizing steps), and it only partially reduced the ADP even when applied at relatively high concentrations. While not definitive, our results suggest that at least one component of the ADP response in Blanes cells is mediated by I_{CAN}. Also consistent with the I_{CAN} hypothesis is our observation that uncaging Ca in Blanes cells activates an inward current that reverses polarity near 0 mV (Hall and Delaney, 2002; Partridge et al., 1994). Interestingly, the voltage dependence that we observed when we activated I_{CAN} directly through photolysis of NP-EGTA in Blanes cells was not as pronounced as the voltage dependence of the ADP activated by depolarizing steps. The different degree of voltage dependence we found in these two protocols may reflect the functional effects of other currents besides I_{CAN} that are activated by the depolarizing step and which oppose the ADP at hyperpolarized membrane potentials.

Interestingly, olfactory granule cells in semi-intact frog forebrain also appear to have I_{CAN}-mediated afterdepolarizations (Hall and Delaney, 2002). The presence of large AHPs in rat granule cells recorded in in vitro brain slices may reflect the absence of tonic cholinergic input to the olfactory bulb; in many brain regions, AHPs evoked by bursts of action potentials are blocked following muscarinic receptor activation (Egorov et al., 2002; Haj-Dahmane and Andrade, 1999). Our preliminary data suggest that this is also true for granule cells in the rat olfactory bulb and that bath perfusion with carbachol can reveal latent ADP responses in granule cells (T. Inoue, R.T.P., and B.W.S., unpublished data).

While the afterdepolarization is likely necessary to initiate persistent firing, the cellular mechanism that maintains persistent firing in Blanes cells appears to rely on triggering a stable intrinsic up state. Several lines of evidence suggest that a Ca-dependent process is necessary to initiate the persistent firing up state in Blanes cells. We found that increasing intracellular Ca by photolysis of NP-EGTA triggered persistent firing, while manipulations that blocked Ca accumulations blocked persistent firing initiated by transient depolarization of Blanes cells. Surprisingly, interrupting persistent firing by injecting a 1–6 s duration hyperpolarizing current does not abolish firing when the step is removed. These two results suggest that persistent firing does not result from a simple regenerative system in which Ca influx from one action potential evoked an ADP response that triggered the next spike. Rather, the frequency of persistent firing in Blanes cells appears to be set through other biophysical or signaling systems that remain to be defined. The occasional membrane potential "notches" that are apparent when persistent firing begins to fail suggest that the kinetics of intrinsic spike afterpotentials may help determine the frequency of persistent firing. Periods of persistent firing do not result from a decrease in action potential threshold (data not shown). Rather, persistent firing appears to reflect the presence of a steady depolarizing current. This tonic depolarizing current may be generated through a plateau potential in a distal dendritic compartment, slow Ca-dependent modulation of leak conductances, or I_{CAN} activation by Ca efflux from a subcellular compartment.

Persistent firing in Blanes cells appears to be closely related to a similar phenomenon in entorhinal cortical neurons (Egorov et al., 2002). Entorhinal pyramidal cells generate large AHPs following action potential bursts. When these AHPs are blocked by carbachol, the resulting ADP can trigger persistent firing. Blanes cells lack large AHP responses and exhibit persistent firing under normal pharmacological conditions. Initiation of persistent firing in entorhinal neurons is blocked by FFA (Egorov et al., 2002), suggesting that the I_{CAN} current responsible for the ADP may contribute to the persistent firing up state. Unlike Blanes cells, entorhinal neurons can fire persistently at different frequencies; strong depolarizing or hyperpolarizing current steps can increase or decrease firing frequency. The underlying intrinsic mechanism that allows Blanes cells (and perhaps entorhinal cells) to fire persistently appears to be distinct from the synaptic mechanisms that mediate prolonged periods of activity in neocortical neurons (McCormick et al., 2003; Sanchez-Vives and McCormick, 2000). These neocortical up states are driven by barrages of excitatory synaptic input and periodically alternate with intervals in which the membrane potential is hyperpolarized. Persistent firing in entorhinal pyramidal cells (Egorov et al., 2002) and olfactory Blanes cells appears to operate at a single-cell level and is insensitive to antagonists of excitatory neurotransmitter receptors.

Functional Significance of Blanes Cells and Persistent Firing in the Olfactory Bulb

Our study demonstrates that Blanes cells represent a new class of bulbar interneurons that inhibit granule cells by releasing GABA from axon terminals. There have been no previous reports of local circuit synaptic responses mediated by axonal transmitter release from interneurons located in the mitral or granule cell layers of the olfactory bulb. Blanes cells may regulate the output cells of the olfactory bulb through at least three mechanisms. First, Blanes cells mediate feedforward inhibition onto granule cells (Figures 3, 7E, and 9B–9D) and thus are in a position to control mitral and tufted cell activity through disinhibition. We directly demonstrated that the same synaptic stimuli that

triggered persistent firing in Blanes cells evoked tonic $GABA_A$ receptor-mediated inhibition onto granule cells. These inhibitory barrages onto granule cells are unlikely to result from persistent activation of mitral cells, as we have previously shown that mitral cells do not receive prolonged excitation following trains of GCL stimuli (Halabisky and Strowbridge, 2003). The close similarity between the frequency of persistent firing in Blanes cells and spontaneous IPSCs in granule cells strongly suggests that these inhibitory barrages arose from one or a small population of activated Blanes cells. We also showed directly that persistent firing in a Blanes cells evoked a persistent train of inhibitory synaptic responses in monosynaptically coupled granule cells. Periodic inhibitory barrages had powerful effects on granule cell excitability and reduced the average number of action potentials triggered by a test stimulus by half. Our results suggest that Blanes cells play an important role in regulating the excitability of inhibitory granule cells and therefore are well positioned to control the strength of recurrent and lateral inhibition onto mitral and tufted cells. Next, Blanes cells also can influence activity in the olfactory bulb by regulating activation (or inactivation) of active currents in granule cells. Inhibitory postsynaptic potentials in granule cells may interact with voltage-dependent Ca currents expressed by these currents. Recently, Egger et al. (Egger et al., 2003) demonstrated that granule cells express low-threshold T-type Ca currents. In other cell types, GABAergic IPSPs can generate rebound discharges by deinactivating T-type Ca currents (McCormick and Bal, 1997). Additional studies will be required to determine whether Blanes cell-mediated IPSPs play a similar role in olfactory granule cells. Finally, because Blanes cells may potentially innervate hundreds of granule cells, spiking activity in Blanes cells may represent a novel mechanism to generate synchronous activity in subpopulations of olfactory bulb neurons. Synchronization may result from correlated rhythmic inhibition of large groups of granule cells activity, which then could lead to synchronization of mitral and tufted cells through periodic disinhibition or by triggering rebound spikes.

Persistent firing in Blanes cells is likely to have several consequences within the olfactory bulb. Persistent firing can be triggered by single shocks to the glomular layer, tetanic extracellular stimulation in the granule cell layer, or by direct depolarization. Slow phasic EPSP-like waveforms (Balu et al., 2004; Halabisky and Strowbridge, 2003), similar to the membrane potential oscillations recorded in mitral and granule cells during normal respiration (Cang and Isaacson, 2003; Margrie and Schaefer, 2003), also are an effective trigger for persistent firing (R.T.P. and B.W.S., unpublished data). Persistent activation of Blanes cells triggered by sensory stimulation will activate tonic feedforward inhibition onto granule cells and is likely to dampen granule cell responses on subsequent respiratory cycles. Cang and Isaacson (2003) observed a sudden damping of granule cell responses following the initial inspiration cycle. It is not clear from these studies whether this effect, which is not observed in mitral cells, reflects persistent activation of Blanes cells or is due instead to intrinsic properties or signaling events in granule cells. Persistent activity also may represent a mechanism for recording short-term events, such as strong transient activation of a specific glomular-linked circuit, within the network dynamics of the olfactory bulb. Friedman and Strowbridge (2003) found that repetitive tetanic stimulation of olfactory bulb slices caused a long lasting increase in oscillatory activity. These persistent oscillations, which were broadly tuned and centered in the γ band, were reflected in both field potential recordings and in an increase in tonic inhibitory input to mitral cells. Because this form of tetanic stimulation is an effective trigger for persistent firing in Blanes cells, it is intriguing to speculate that activity in these cells may contribute to these network oscillations.

Persistent firing in Blanes cells is remarkably robust. Even strong hyperpolarizing membrane steps (50 mV for 2–3 s) did not abolish persistent firing, suggesting that, once initiated, persistent firing is likely to be unaffected by subsequent inhibitory synaptic inputs. Prolonged hyperpolarization (60 s) did block persistent firing, but it is unclear whether barrages of hyperpolarizing inputs would ever be presented to Blanes cells over this long duration. Rather, it seems likely that under physiological conditions, persistent firing is limited by the duration of periodic sensory stimuli that summate to bring the membrane potential within the membrane potential window where persistent firing is possible. The prolonged EPSPs triggered in Blanes cells by single glomerular layer shocks (Figure 9A) suggest that an inspiration-like pattern of excitation will exhibit a large degree of temporal summation, perhaps allowing Blanes cells to maintain their firing between inspiration cycles.

Experimental Procedures

Olfactory bulb slices (300 μm thick) from P14–P24 Sprague-Dawley rats were made using a modified Leica (Nussloch, Germany) VT1000S vibratome as previously described (Friedman and Strowbridge, 2003; Isaacson and Strowbridge, 1998). An artificial cerebrospinal fluid (ACSF) solution with reduced Ca was used when preparing and storing slices. This solution contained 124 mM NaCl, 2.6 mM KCl, 1.23 mM NaH_2PO_4, 3 mM $MgSO_4$, 26 mM $NaHCO_3$, 10 mM dextrose, and 1 mM $CaCl_2$, equilibrated with 95% O_2/5% CO_2 and was chilled to 4ºC during slicing. Olfactory bulb slices were incubated in a 30ºC water bath for 30 min and then maintained at room temperature. During experiments, olfactory bulb slices were superfused with ACSF that contained 124 mM NaCl, 3 mM KCl, 1.23 mM NaH_2PO_4, 1.2 mM $MgSO_4$, 26 mM $NaHCO_3$, 10 mM dextrose, and 2.5 mM $CaCl_2$, equilibrated with 95% O_2/5% CO_2 and warmed to 30ºC. All drugs except for TTX (Calbiochem) and *o*–nitrophenyl EGTA (NP-EGTA, Molecular Probes) were obtained from Sigma (St. Louis, MO).

Whole-cell current-clamp recordings were made from olfactory neurons visualized with infrared-differential interference contrast (IR-DIC) optics using either Axioskop 1 FS (Carl Zeiss) or BX51WI (Olympus) fixed-stage upright microscopes and either Axopatch 1D or Axoclamp 2B amplifiers (Axon instruments). Electrodes used for whole-cell recordings (5–7 MΩ) were pulled from thin-wall capillary tubes with filament (WPI) and contained 140 mM K-methylsulfate, 4 mM NaCl, 10 mM HEPES, 0.2 mM EGTA, 4 mM MgATP, 0.3 mM Na_3GTP, 10 mM phosphocreatine for current-clamp experiments, and 115 mM Cs-methanesulfonate, 25 mM TEA-methanesulfonate, 10 mM HEPES, 5 mM QX-314, 4 mM NaCl, 4 mM MgATP, 1 mM EGTA, 0.3 mM Na_3GTP, 10 mM phosphocreatine for voltage-clamp recordings in granule cells. In several experiments, the EGTA concentration was raised to 10 mM to increase Ca buffering capacity.

In the experiments shown in Figures 5C and 5D, we used a different internal solution for Ca uncaging under voltage-clamp conditions (118 mM Cs-methanesulfonate, 25 mM TEA-methanesulfonate,

10 mM HEPES, 4 mM NaCl, 4 mM MgATP, 0.3 mM Na_3GTP, 10 mM phosphocreatine, 2 mM NP-EGTA) and an external solution that contained TTX (1 μM). Control responses (Figure 5C_2) were obtained using the same internal solution with no added NP-EGTA. The Ca uncaging results shown in Figure 7D were obtained using a current-clamp internal solution (140 mM K-methanesulfonate, 8 mM NaCl, 10 mM HEPES, 4 mM MgATP, 0.3 mM NaGTP, 10 mM phosphocreatine, 2 mM NP-EGTA.) We used a 150 W Xe short-arc lamp (OptiQuip) controlled by a fast electronic shutter (Uniblitz) to photolyse NP-EGTA (Ellis-Davies and Kaplin, 1994), which was loaded by one to three depolarizing steps to 0 mV (400 ms duration) immediately before the exposure. The output of the Xe lamp was directed toward the microscope objective (Zeiss 63× water-immersion, NA = 0.9) using a long-pass dichroic mirror designed for epifluorescent detection of fura-2 (400DCLP, Omega Optical). In most experiments, we used arc lamp exposures of 100–2000 ms focused on the cell body region to activate Ca-dependent responses.

Neurons were visualized with either the ABC peroxidase method (Horikawa and Armstrong, 1988) following intracellular Neurobiotin labeling (0.5%) and paraformaldehyde fixation or by using two-photon imaging in living slices following intracellular labeling with Alexa 594 (100 μM; Molecular Probes). We used the Neurolucida (Microbrightfield) to generate the neuronal reconstructions shown in Figure 1C and the morphometric data in Figure 1D. Live imaging experiments utilized a custom two-photon microscope based on the Verdi V10 pump laser, Mira 900 Ti-sapphire laser (both from Coherent, Santa Clara, CA) and a high-speed XY galvanometer mirror system (6210; Cambridge Technology). Intracellularly loaded fluorescent dyes were excited at 830 nm through a 60× water-immersion objective (Olympus). Emitted light was detected through a light path that included a 700DCLPXR dichroic mirror, a BG39 emission filter (both from Chroma Technology), and a cooled PMT detector module (H7422P-40; Hamamastu). Photomultiplier output was converted into an analog voltage by a high-bandwidth current preamplifier (SR-570; Stanford Research Systems). Custom Visual Basic software written by BWS controlled the scanning system and image analysis functions. Laser beam intensity was controlled electronically through a Pockels cell attenuator (ConOptics) and a shutter (Uniblitz). In most experiments, the output of the Mira laser was attenuated by 90%–95%.

We used two-photon microscopy to facilitate paired recordings by first recording from the presynaptic neuron with an electrode containing Alexa 594 (100 μM, Molecular Probes). After waiting 20–25 min for the dye to diffuse through distal processes, we used a fast scanning mode (3000 lines per second) to identify the axon (the nontapering, spineless process that typical emerged from one of the primary dendrites of the Blanes cell) and to follow this process until it started to bifurcate. In most cells, we could readily identify the axonal plexus within 30–40 min after forming a whole-cell recording on the Blanes cell. We then were able to record from between 1 and 5 potential target cells in this region before mechanical movements caused by repeated placements of the patch-clamp electrode deteriorated the Blanes cell recording. We determined whether postsynaptic responses evoked by Blanes cell action potentials were monosynaptic by measuring IPSP onset latency; monosynaptic responses had short, relatively invariant onset latencies that varied between 0.8 and 2.2 ms. All monosynaptic Blanes-to-granule cell monosynaptic IPSPs that we recorded also had high unitary probability (>90% assessed by single action potentials evoked in the Blanes cell every 2 s.)

Series resistance was typically <15 MΩ and was routinely compensated by >80% in voltage-clamp experiments. Inhibitory postsynaptic currents were recorded in granule cells at a holding potential of 0 mV in the experiment shown in Figure 9C to minimize the amplitude of spontaneous EPSCs. Voltage and current records were low-pass filtered at 2 kHz and sampled at 5 kHz using a ITC-18 16-bit analog-to-digital converter (Instrutech) using custom software written in Visual Basic 6 (Microsoft). Origin 7.5 (OriginLab) and custom Visual Basic routines were used to analyze data. Synaptic responses were evoked using either tungsten monopolar electrodes (FHC) connected to a constant-current stimulus isolation unit (WPI) or by directly activating a presynaptic neuron. We determined the average amplitude of GCL-evoked EPSPs onto Blanes cells using minimal stimulation and averaging the response amplitude in nonfailure trials. Pharmacological agents were applied by switching the perfusion solution. Voltages presented are not corrected for the liquid junction potential. Statistical significance was determined using the Student's t test. Data are presented as mean ± SEM.

Acknowledgments

We thank Ramani Balu and Diana Kunze for helpful discussions related to this project. This study was supported by NIH grant DC04285 to B.W.S.; R.T.P. received support from NIH training grant AG00271. We are grateful to C.J. Frazier and S. Jones for constructive comments on this manuscript.

Received: May 2, 2005
Revised: December 21, 2005
Accepted: February 9, 2006
Published: March 15, 2006

References

Alonso, J.R., Brinon, J.G., Crespo, C., Bravo, I.G., Arevalo, R., and Aijon, J. (2001). Chemical organization of the macaque monkey olfactory bulb: II. Calretinin, calbindin D-28k, parvalbumin, and neurocalcin immunoreactivity. J. Comp. Neurol. *432*, 389–407.

Aungst, J.L., Heyward, P.M., Puche, A.C., Karnup, S.V., Hayar, A., Szabo, G., and Shipley, M.T. (2003). Centre-surround inhibition among olfactory bulb glomeruli. Nature *426*, 623–629.

Balu, R., Larimer, P., and Strowbridge, B.W. (2004). Phasic stimuli evoke precisely timed spikes in intermittently discharging mitral cells. J. Neurophysiol. *92*, 743–753.

Blanes, T. (1898). Sobre algunos puntos dudoses de la estructura del bulbo olfatorio. Revta Trimest Microgr. *3*, 99–127.

Bourque, C.W. (1986). Calcium-dependent spike after-current induces burst firing in magnocellular neurosecretory cells. Neurosci. Lett. *70*, 204–209.

Cang, J., and Isaacson, J.S. (2003). In vivo whole-cell recording of odor-evoked synaptic transmission in the rat olfactory bulb. J. Neurosci. *23*, 4108–4116.

Douglas, R.J., and Martin, K.A. (1991). A functional microcircuit for cat visual cortex. J. Physiol. *440*, 735–769.

Egger, V., Svoboda, K., and Mainen, Z.F. (2003). Mechanisms of lateral inhibition in the olfactory bulb: efficiency and modulation of spike-evoked calcium influx into granule cells. J. Neurosci. *23*, 7551–7558.

Egorov, A.V., Hamam, B.N., Fransen, E., Hasselmo, M.E., and Alonso, A.A. (2002). Graded persistent activity in entorhinal cortex neurons. Nature *420*, 173–178.

Ellis-Davies, G.C., and Kaplin, J.H. (1994). Nitrophenyl-EGTA, a photolabile chelator that selectively binds Ca2+ with high affinity and releases it rapidly upon photolysis. Proc. Natl. Acad. Sci. USA *91*, 187–191.

Friedman, D., and Strowbridge, B.W. (2003). Both electrical and chemical synapses mediate fast network oscillations in the olfactory bulb. J. Neurophysiol. *89*, 2601–2610.

Ghamari-Langroudi, M., and Bourque, C.W. (2002). Flufenamic acid blocks depolarizing afterpotentials and phasic firing in rat supraoptic neurones. J. Physiol. *545*, 537–542.

Gracia-Llanes, F.J., Crespo, C., Blasco-Ibanez, J.M., Marques-Mari, A.I., and Martinez-Guijarro, F.J. (2003). VIP-containing deep short-axon cells of the olfactory bulb innervate interneurons different from granule cells. Eur. J. Neurosci. *18*, 1751–1763.

Haj-Dahmane, S., and Andrade, R. (1998). Ionic mechanism of the slow afterdepolarization induced by muscarinic receptor activation in rat prefrontal cortex. J. Neurophysiol. *80*, 1197–1210.

Haj-Dahmane, S., and Andrade, R. (1999). Muscarinic receptors regulate two different calcium-dependent non-selective cation currents in rat prefrontal cortex. Eur. J. Neurosci. *11*, 1973–1980.

Halabisky, B., and Strowbridge, B.W. (2003). Gamma-frequency excitatory input to granule cells facilitates dendrodendritic inhibition in the rat olfactory Bulb. J. Neurophysiol. *90*, 644–654.

Hall, B.J., and Delaney, K.R. (2002). Contribution of a calcium-activated non-specific conductance to NMDA receptor-mediated synaptic potentials in granule cells of the frog olfactory bulb. J. Physiol. *543*, 819–834.

Horikawa, K., and Armstrong, W.E. (1988). A versatile means of intracellular labeling: injection of biocytin and its detection with avidin conjugates. J. Neurosci. Methods *25*, 1–11.

Isaacson, J.S., and Strowbridge, B.W. (1998). Olfactory reciprocal synapses: dendritic signaling in the CNS. Neuron *20*, 749–761.

Jahr, C.E., and Nicoll, R.A. (1980). Dendrodendritic inhibition: demonstration with intracellular recording. Science *207*, 1473–1475.

Kakuta, S., Oda, S., Takayanagi, M., and Kishi, K. (1998). Parvalbumin immunoreactive neurons in the main olfactory bulb of the house musk shrew, Suncus murinus. Brain Behav. Evol. *52*, 285–291.

Li, Z., and Hatton, G.I. (1997). Reduced outward K+ conductances generate depolarizing after-potentials in rat supraoptic nucleus neurones. J. Physiol. *505*, 95–106.

Lopez-Mascaraque, L., De Carlos, J.A., and Valverde, F. (1986). Structure of the olfactory bulb of the hedgehog (Erinaceus europaeus): description of cell types in the granular layer. J. Comp. Neurol. *253*, 135–152.

Margrie, T.W., and Schaefer, A.T. (2003). Theta oscillation coupled spike latencies yield computational vigour in a mammalian sensory system. J. Physiol. *546*, 363–374.

McCormick, D.A., and Bal, T. (1997). Sleep and arousal: thalamocortical mechanisms. Annu. Rev. Neurosci. *20*, 185–215.

McCormick, D.A., Shu, Y., Hasenstaub, A., Sanchez-Vives, M., Badoual, M., and Bal, T. (2003). Persistent cortical activity: mechanisms of generation and effects on neuronal excitability. Cereb. Cortex *13*, 1219–1231.

Mori, K., Nagao, H., and Yoshihara, Y. (1999). The olfactory bulb: coding and processing of odor molecule information. Science *286*, 711–715.

Nakajima, T., Okamura, M., Ogawa, K., and Taniguchi, K. (1996). Immunohistochemical and enzyme histochemical characteristics of short axon cells in the olfactory bulb of the golden hamster. J. Vet. Med. Sci. *58*, 903–908.

Ohm, T.G., Muller, H., Ulfig, N., and Braak, E. (1990). Glutamic-acid-decarboxylase-and parvalbumin-like-immunoreactive structures in the olfactory bulb of the human adult. J. Comp. Neurol. *291*, 1–8.

Partridge, L.D., and Valenzuela, C.F. (2000). Block of hippocampal CAN channels by flufenamate. Brain Res. *867*, 143–148.

Partridge, L.D., Muller, T.H., and Swandulla, D. (1994). Calcium-activated non-selective channels in the nervous system. Brain Res. Brain Res. Rev. *19*, 319–325.

Price, J.L., and Powell, T.P. (1970a). The mitral and short axon cells of the olfactory bulb. J. Cell Sci. *7*, 631–651.

Price, J.L., and Powell, T.P. (1970b). The synaptology of the granule cells of the olfactory bulb. J. Cell Sci. *7*, 125–155.

Rall, W., and Shepherd, G.M. (1968). Theoretical reconstruction of field potentials and dendrodendritic synaptic interactions in olfactory bulb. J. Neurophysiol. *31*, 884–915.

Rall, W., Shepherd, G.M., Reese, T.S., and Brightman, M.W. (1966). Dendrodendritic synaptic pathway for inhibition in the olfactory bulb. Exp. Neurol. *14*, 44–56.

Roper, P., Callaway, J., Shevchenko, T., Teruyama, R., and Armstrong, W. (2003). AHP's, HAP's and DAP's: how potassium currents regulate the excitability of rat supraoptic neurones. J. Comput. Neurosci. *15*, 367–389.

Roper, P., Callaway, J., and Armstrong, W. (2004). Burst initiation and termination in phasic vasopressin cells of the rat supraoptic nucleus: a combined mathematical, electrical, and calcium fluorescence study. J. Neurosci. *24*, 4818–4831.

Sanchez-Vives, M.V., and McCormick, D.A. (2000). Cellular and network mechanisms of rhythmic recurrent activity in neocortex. Nat. Neurosci. *3*, 1027–1034.

Schneider, S.P., and Macrides, F. (1978). Laminar distributions of internuerons in the main olfactory bulb of the adult hamster. Brain Res. Bull. *3*, 73–82.

Schoppa, N.E., Kinzie, J.M., Sahara, Y., Segerson, T.P., and Westbrook, G.L. (1998). Dendrodendritic inhibition in the olfactory bulb is driven by NMDA receptors. J. Neurosci. *18*, 6790–6802.

Scott, J.W., McDonald, J.K., and Pemberton, J.L. (1987). Short axon cells of the rat olfactory bulb display NADPH-diaphorase activity, neuropeptide Y-like immunoreactivity, and somatostatin-like immunoreactivity. J. Comp. Neurol. *260*, 378–391.

Shepherd, G.M., and Greer, C.A. (1998). Olfactory Bulb. In Synaptic Organization of the Brain, G.M. Shepherd, ed. (New York: Oxford University Press), pp. 159–204.

Stepanyants, A., Tamas, G., and Chklovskii, D.B. (2004). Class-specific features of neuronal wiring. Neuron *43*, 251–259.